Molecular Dynamics Simulations of the Effect of the Composition of Calcium Alumino-Silicate Intergranular Films on Alumina Grain Growth

Shenghong Zhang and Stephen H. Garofalini*

Interfacial Molecular Science Laboratory, Department of Materials Science and Engineering, Rutgers University, Piscataway, New Jersey, 08855

Received: June 9, 2005; In Final Form: August 23, 2005

Molecular dynamics simulations were performed to study the effect of the composition of the intergranular film (IGF) on anisotropic and isotropic grain growth in α-Al_2O_3. In the simulations, the IGF is formed while in contact with two differently oriented alumina crystals, with the alumina (0001) basal plane on one side and the $(11\bar{2}0)$ prism plane on the other. Five different compositions in the IGFs were studied. Results show preferential growth along the $[11\bar{2}0]$ of the $(11\bar{2}0)$ surface in comparison to growth along the [0001] direction on the (0001) surface for compositions near a Ca/Al ratio of 0.5. Such preferential growth is consistent with anisotropic grain growth in alumina, where platelets form because of faster growth of the prism orientations than the basal orientation. The simulations also show the mechanism by which Ca ions in the IGF inhibit growth on the basal surface. At compositions with high or low Ca/Al ratios, growth along each surface normal is equivalent, indicating isotropic grain growth, although the attachment rates are quite different, which may indicate differences between normal grain growth and abnormal, but isotropic, grain growth. The simulations provide an atomistic view of attachment onto crystal surfaces, affecting grain growth in alumina.

Introduction

Alumina ceramic is an important industrial material in many applications for its high hardness, corrosion resistance, and low thermal expansion coefficient. The green compacts and the sintering procedures have great effects on the structure and mechanical properties of the final products. Furthermore, to improve other mechanical properties such as low fracture toughness and poor thermal shock resistance, one or several doping materials are added to get the desired results.

Amorphous intergranular films present between liquid-sintered alumina grains and nonpure alumina sintering processes introduce Ca, Si, and other impurities.[1−3] Many experiments show that there are significant differences in the final structure and mechanical properties between the pure (greater than 99.99%) and the doped alumina ceramics.[4] For pure Al_2O_3 sintered in clean conditions, normal and continuous grain growth is found, following normal grain growth kinetics. The final sintered structure is homogeneous and only equiaxed grains are found experimentally.[5] However, when commercial alumina is used or some sintering aids (like Si, Ca, Mg, and other cations) are added into the pure alumina before the sintering process, grain growth behavior changes and the microstructure of the grains and grain boundaries vary from the pure conditions. Not only is the grain growth dependent on the purity of the alumina and the sintering conditions but densification is also affected. Experimental results show that lattice diffusion dominates the densification under clean conditions while lattice and grain-boundary diffusion both contribute to the densification under normal sintering conditions.[6]

Some experiments show that abnormal grain growth (AGG) is not found at the initial stage of the sintering while the grain size is quite small but grain size in itself is not the reason for AGG.[4] Even in the sintering of pure alumina, AGG was observed after a very long sintering time because the contaminant cannot be avoided completely. AGG is not an intrinsic property of alumina but an extrinsic property that is controlled by the impurities or contaminants.[7] However, impurity species in alumina have a different effect on AGG. It is well accepted that the presence of Ca and Si at the grain boundary triggers AGG, while Mg inhibits AGG in alumina sintering.[8−12] Platelike crystals form large, flat basal surfaces with thin intergranular films when AGG happens.[13] Because of the possible uneven distribution of a small amount of liquid between grain boundaries and triple points, Kolar suggested that the coexistence of both wet and dry boundaries may bring about AGG.[14] After investigating four commercial alumina powders, Cho et al. proposed that chemical inhomogeneity is the reason for AGG because they found that, in such alumina, a relatively small portion of coarse particles in all powders contains a significantly high concentration of impurities.[15] On the other hand, by comparing the alumina crystal shape with AGG experimentally, the basal planes were found to be very smooth and flat while the prism planes were rough.[16] The energy barrier for the attachment to the rough surface is negligible compared to that on the smooth flat surface in the coarsening process controlled by interface diffusion. So only very large grains would gain enough driving force for the nucleation on the flat surface and then coarsening could happen. Because the coarsening caused by 2-D nucleation will show a discontinuous grain growth behavior in different orientation planes, Lee suggested that the nucleation process at different planes is the reason for the AGG.[16] In the Kwon et al. experiments, the appearance of the liquid phase (IGF) was thought to increase the boundary mobility and AGG is explained as a result of the enhanced growth on the nonbasal plane due to the re-entrant edges formed at the grain boundaries.[17]

* To whom correspondence should be addressed. E-mail: shg@glass.rutgers.edu.

10.1021/jp0531053 CCC: $33.50
Published on Web 01/20/2006

Experiments also show that significant segregation of Ca and other cations at the alumina grain boundaries happens while such impurities are still below the solid solution limits in the grains.[9] The segregation of calcium is anisotropic for different orientations of alumina. Bae and Baik showed that low concentrations of either calcia or silica in the IGF or smaller combinations of both together cause AGG in alumina.[6] It is very hard to study the atomic structure of the IGF in polycrystalline ceramics experimentally because of the extremely thin and amorphous structures of these films, although there has been recent success in studies of IGFs in Si_3N_4.[18−20] It is proposed that an IGF should have a stable equilibrium thickness on the order of several nanometers,[21] although the structure of such a thin glass between crystals should be different than the bulk glass analogue because of the influence of contact with the crystal surfaces.

Considering bulk glass structure, Al ions in silicate glasses occupy tetrahedral sites, as opposed to the octahedral sites in α-Al_2O_3. In order for this to occur, a charge-compensating cation is usually associated with the AlO_4^- site. Tetrahedral Al is also observed in siliceous zeolites. With a sufficient concentration of Ca in the IGF to charge compensate two Al for each Ca, the Al ions can remain tetrahedrally coordinated (to maintain the silicate glass network structure). Excess CaO (R = [Ca]/[Al] > 0.5) in a silicate glass would cause the formation of so-called nonbridging oxygens (NBOs), which are singly coordinated to a strong network former (such as Si) and less strongly bonded to the network modifier (Ca). (A brief discussion of the role of Al and modifier ions in silicate glasses using alkali aluminosilicates is available in ref 22 and references therein.) As related to the IGF in contact with a basal oriented alumina surface, any Ca in excess of the charge equivalence point (R_e = [Ca]/[Al] = 0.5) would mean either formation of NBO in the IGF or segregation of the Ca to the basal crystal surface to charge compensate undercoordinated O present at the surface.[23] The combination of NBO in the IGF glass and undercoordinated O in the crystal lattice surface is energetically less favorable than no NBOs in the glass and no undercoordinated O in the surface. The latter situation was the case in our earlier study of IGF compositions,[23,24] where Ca ions preferentially segregated to the alumina basal crystal surface. However, with increasing amounts of alumina in excess of the CaO equivalence (R < R_e), behavior might change.

Our previous simulations of amorphous silicate IGFs in contact with alumina crystals and silicon nitride crystals clearly showed ordered structures at the interfaces and density oscillations into the IGF induced by the crystals.[23−28] Recent high-resolution TEM (HRTEM) studies observe such density oscillations.[20] These density oscillations decay within 1 nm of the interface, attaining a glassy structure in the interior of the thicker films. Most importantly, the previous simulations of IGFs between the differently oriented crystals showed anisotropic growth.[24,27] "Growth" in our discussion means adsorption of species from the IGF onto the crystal surface consistent with the crystal orientation and composition such that the crystal lattice extends along the surface normal of the particular plane in contact with the IGF. In the nitride case, growth along the basal surface normal was more rapid than that along the prism surface normal. In the alumina case, the simulations showed preferential growth along the $[11\bar{2}0]$ direction on the $(11\bar{2}0)$ oriented crystal and no such growth in the [0001] direction on the basal crystal. Both results are consistent with anisotropic grain growth in the respective systems seen experimentally. Concerning the alumina system, the presence of Ca ions in the IGF affected adsorption of Al ions from the IGF onto the crystal lattice sites on the (0001) surface creates the anisotropy in growth behavior. However, experimental data clearly shows that normal grain growth occurs in the alumina system, so composition of the IGF must play an important role. In this paper, higher concentrations of Al in the IGF (R < 0.5) than those previously considered are used to evaluate growth behavior.

TABLE 1: Parameters for Modified BMH Pair Potential

atom pair	A_{ij} (fJ)	β_{ij} (pm)	ρ_{ij} (pm)
O−O	0.0725	234	29
Si−Si	0.1877	230	29
Al−Al	0.0500	235	29
Ca−Ca	0.7000	230	29
Si−Al	0.2523	233	29
Si−Ca	0.2215	230	29
Al−Ca	0.2178	230	29
Si−O	0.2962	234	29
Al−O	0.2490	234	29
Ca−O	0.5700	234	29

Computer Procedures. Similar to previous studies,[23−25,29−31] a multibody interatomic potential was used in the simulations and is given as

$$V = \sum_{i \neq j} V_{ij}^{\mathrm{BMH}} + \sum_{i \neq j \neq k} V_{jik}^{3-\mathrm{body}} \tag{1}$$

where V_{ij}^{BMH} is the pairwise modified BMH potential term and $V_{jik}^{3-\mathrm{body}}$ is the 3-body potential term. The modified BMH potential is defined as

$$V_{ij}^{\mathrm{BMH}} = A_{ij} \exp\left(\frac{-r_{ij}}{\rho_{ij}}\right) + \frac{z_i z_j e^2}{r_{ij}} erfc\left(\frac{r_{ij}}{\beta_{ij}}\right) \tag{2}$$

The first term is the repulsion term in the modified BMH pair potential and represents the core electron overlap when the two atoms get too close; the second term is a screened Coulombic interaction. r_{ij} is the separation distance between the ions i and j, z_i and z_j are the formal charge of the ions, and β_{ij} is a species-dependent term that reduces the formal charges as a function of distance between the ij pair. The values for the parameters A_{ij}, β_{ij}, and ρ_{ij} of each pair type were determined in this lab and previously presented[23,24,30] (see Table 1). Atomic charges for the silicon, oxygen, aluminum, and calcium ions are +4, −2, +3, and +2, respectively.

The partial covalent bonding of the species has preferred bonding angles at which the bonded species have the lowest energy. When the bonding angle deviates from the preferred one, the energy will increase. The 3-body potential accounts for this effect by raising the energy on a central ion within a triplet as the angle deviates from an ideal angle. The 3-body potentials applied to all Si, O, and Al ions as central ions i are given as

$$V_{jik}^{3-\mathrm{body}} = \lambda_{jik} \exp\left(\frac{\gamma_{ij}}{r_{ij} - r_{ij}^0} + \frac{\gamma_{ik}}{r_{ik} - r_{ik}^0}\right) \Omega_{jik} \tag{3}$$

when $r_{ij} < r_{ij}^0$ and $r_{ik} < r_{ik}^0$. Otherwise, $V_{jik}^{3-\mathrm{body}} = 0$ when $r_{ij} > r_{ij}^0$ or $r_{ik} > r_{ik}^0$.

The angular part, Ω_{jik}, is given as

$$\Omega_{jik} = (\cos\theta_{jik} - \cos\theta_{jik}^0)^2 \tag{4}$$

for the Si/Al−O−Si/Al and O−Si−O structure, while for the O−Al−O triplet, it is defined as

$$\Omega_{jik} = [(\cos\theta_{jik} - \cos\theta^0_{jik})\sin\theta_{jik}\cos\theta_{jik}]^2 \qquad (5)$$

where the three atoms form angle θ_{jik} with the central atoms as the vertex *i* in these triplets for both conditions. Since Ca is considered mainly ionic, no 3-body potential centered on Ca as ions *i* in the *jik* triplet is used. The parameters, shown in Table 2, were also developed in previous studies.[25,30,32,33]

Previous simulations using this potential and parameters generated stable crystals of both α-Al_2O_3 and γ-Al_2O_3,[30] where the coordination of the Al ions differs. Surface energies were calculated, with results providing an explanation for the stability of small crystals of γ-Al_2O_3 in comparison to α-Al_2O_3. Relevant to the current work, simulations of the surface structure and energy of α-Al_2O_3 showed that the single Al termination plane of the basal orientation is the lowest energy configuration,[30] consistent with previous shell model calculations and subsequent ab initio DFT calculations (all near 2 ± 0.5 J/m^2).[34,35] The single O termination layer for the (11$\bar{2}$0) gave a slightly higher surface energy. Simulations of silicate glasses using this potential also reproduce experimental data.[32,33,36,37]

Five calcium alumino-silicate IGF compositions were chosen for the current work. They are identified by their species ratios ($CaO:Al_2O_3:SiO_2$) and are given in Table 3, along with system sizes. The glassy IGFs were made between two dissimilar α-alumina orientations, the (0001) and (11$\bar{2}$0), creating a ((0001) oriented crystal)/(IGF)/((11$\bar{2}$0) oriented crystal) system. A schematic drawing of the system is shown in Figure 1. The simulation procedure is the same as that previously published,[24] where it is discussed in detail. The only difference is that different IGF compositions are studied here.

Briefly, each crystal is aligned such that the appropriate crystal terminating plane would be in contact with the IGF, as shown in Figure 1. The atoms in the top few layers of the upper crystal and the bottom layers of the lower crystal are always frozen so that periodic boundaries can be used in all three dimensions. That is allowed because these frozen atoms are never central atoms in the potentials, so they never "see" each other, although they can act as neighbors (j) to the mobile atoms. Previous simulations have shown that the effect of frozen atoms ~2 nm away from the surfaces have no effect on the surface structure.[38]

The glassy IGFs are made between the crystals by randomly inserting the atoms of the IGF composition in the volume between the crystals, followed by a melt/quench procedure shown in Table 4. Both NVE and NPT simulations are used, and a time step of 1×10^{-15} s is used throughout the simulations. To minimize interface mixing and roughening, the crystal atoms do not respond to the interatomic forces at the high melt temperatures. While dissolution and reprecipitation of the crystals would be more realistic, the computational time would be prohibitive. In addition, the roughened interface would be considerably less amenable to subsequent analysis, and the time required to attain a resmoothed surface might again be computationally prohibitive. At these higher temperatures, the crystal atoms nonetheless do relax en-masse to the external pressure applied in the direction perpendicular to the IGF/crystal interfaces. This procedure allows attainment of the appropriate thickness for the constant number of atoms in the IGF based on the resultant IGF structure. At lower temperatures, all atoms respond to the interatomic forces except those in the frozen layers farthest from the crystal/IGF interfaces, which still moved en-masse to the external pressure. The *x*, *y*, and *z* dimensions are approximately 5.2, 5, and 10 nm, respectively, with the *x* and *y* dimensions changing with the thermal expansion coefficient of the crystal to minimize elastic effects. The IGF is ~4 nm in all simulations. Again, details have been presented elsewhere.[24] In addition, the results from those previous simulations are included here to show the effect of composition of the IGF on growth on the different crystallographic orientations.

TABLE 2: Parameters for 3-Body Potential

atom triplet	λij (fJ)	γ_{ij} (pm)	r^0_{ij} (pm)	θ^0_{jik}
Al/Si−O−Al/Si	0.001	200	260	109.5
O−Al/Si−O	0.024	280	300	109.5

TABLE 3: Composition and System Sizes[a]

	mole ratio	specific number of atoms				
sample no.	$CaO:Al_2O_3:SiO_2$	Ca	Al	Si	O	total
334	3:3:4	720	1440	960	4800	7920
123	1:2:3	400	1600	1200	5200	8400
221	2:2:1	1000	2000	500	5000	8500
121	1:2:1	550	2200	550	4950	8250
141	1:4:1	340	2720	340	5100	8500

[a] The other four compositions included in Figure 5, the 112, 216, 313, and 14 5 35 systems, can be found in ref 24. The number of atoms in the alumina crystals in the simulation are 7920 and 8640 for the basal and prism orientations, respectively.

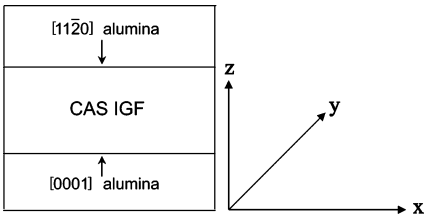

Figure 1. Schematic view of the IGF/crystal system used in this work.

TABLE 4: Melt/Quench Process for Making Glassy IGF between Crystals

quench temperature	conditions	duration
10 000 K	NVE, crystal frozen	10 ps
8000 K	*x* and *y* constant,[a] $P_z = 5$ GPa	20 ps
6000 K	as above	40 ps
4000 K	as above	40 ps
3000 K	*x* and *y* constant,[a] $P_z = 3$ GPa, crystal unfrozen	50 ps
2000 K	NPT, $p = 0.1$ MPa	100 ps
1000 K	as above	100 ps
300 K	as above	20 ps

[a] *x* and *y* dimensions change with thermal expansion coefficient as *T* changes.

Results and Discussion

Snapshots. Similar to previous simulations, the interior portions of the IGF were amorphous.[24] For brevity, they are not shown or discussed in this paper. The thin slabs of ordered structures at the (0001) basal and (11$\bar{2}$0) prism interfaces of two representative systems are shown in Figure 2. The original crystal and the IGF atoms are separated by a solid, straight line in the snapshots, with the crystal atoms below the line. The snapshots of these systems show the evolution of the interface structures for two different IGF compositions. At the basal side, the ordered "cage" structures previously reported are clear and almost fully occupied by Ca ions in the 221 system because of the high Ca concentration in this system. The two Ca ions in a single cage in the 221 basal image are offset by the third dimension into the plane of the image. Ca ions preferentially segregate to the "cage" sites in calcium silicate IGFs,[23] where

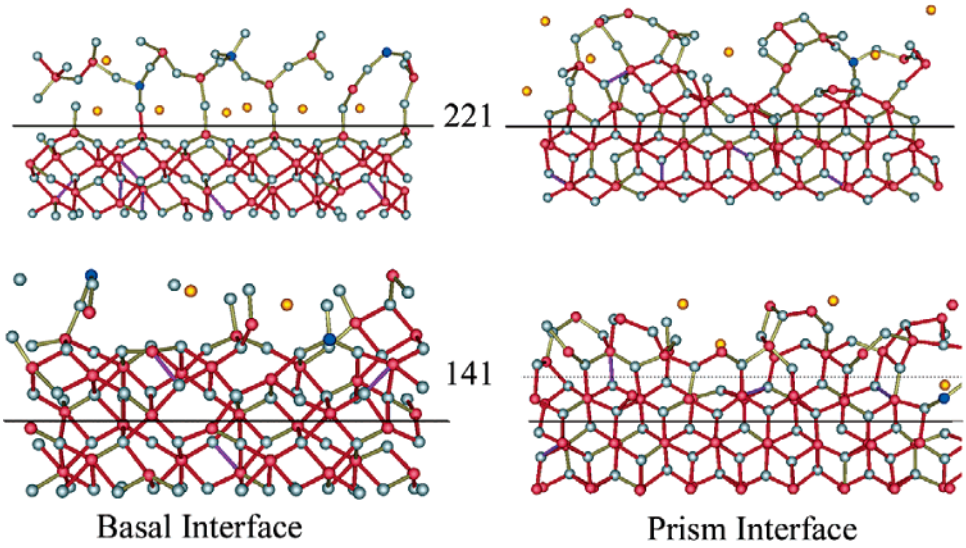

Figure 2. Snapshots of thin cross-sections of atoms into the plane of the page near the basal and prism interfaces of two compositions in the simulations. Atoms from the crystal are below the dark solid horizontal line in each image; atoms originally from the IGF are above the dark horizontal line. Atoms between the dashed line and the solid line in the 141 prism image indicate the degree of ordering of the atoms from the IGF that adsorbed onto the crystal surface, forming an extension of the prism-oriented crystal: Al = red, O = gray, Si = blue, and Ca = yellow. Ca−O bonds are not drawn.

they charge compensate the tetrahedrally coordinated terminal Al on the crystal surface (similar to a zeolitic Al) and the undercoordinated O in the crystal surface. This "cage" structure has been discussed previously.[23,26]

At the prism side, growth of the crystal is observed in both examples, with multiple crystalline layers forming on the prism surface of the 141 system. The atoms above the solid line are from the IGF, and those between the solid line and the dashed line clearly show the growth of the crystal layer in the $[11\bar{2}0]$ direction at this composition. Even the atoms above the dashed line show the beginnings of order similar to the crystal.

Density Profile Analysis. The density profiles of atoms near the basal and prism interfaces for all of the systems studied in this paper are shown in Figure 3. The concentration of Al in the IGF is increasing in the order of 334, 123, 221, 121, and 141. The density profile of atoms in the basal-oriented crystal shows the single O peak and the double Al peaks while that of atoms in the prism-oriented crystal shows the double O peaks and single Al peak, consistent with each crystalline orientation. The lowest surface energy configurations of these crystals are the single Al termination plane for the basal surface and the single O termination plane for the prism surface. Therefore, continuation of each crystal along the specific surface normal of each orientation requires a second Al peak to occur on the basal side, followed by an O peak and a second O peak to occur on the prism side, followed by an Al peak.

Previous simulations showed that Ca ions preferentially adsorbed onto the basal surface in calcium silicate IGF compositions,[23] inhibiting Al adsorption in calcium aluminosilicate IGF compositions.[24,25] This is again the case for most of the compositions studied here, as shown on the left side of Figure 3. At the basal side, for all but the 141 composition, the first adsorbed Al peak from the IGF is much smaller than the terminal Al crystal peak on this side and the first adsorbed Ca peak is present at the same position as the first O peak (indicative of the cage structure shown in Figure 2).

At the equivalence point ($R_e = 0.5$) in the 334 and 221 systems, the first adsorbed Ca peak is larger than that in the other compositions and the first adsorbed Al peak adjacent to the basal surface is smaller than that in the other compositions which have excess Al ($R < R_e$) in the IGF. In the 334 and 221 systems, one might anticipate that Ca and Al would remain equally associated within the IGF (as would be the case in a silicate glass). However, the presence of the crystal surfaces modifies this behavior, and as seen in all of the compositions, a very strong second adsorbed Al peak forms on the basal side (which is at the "top" of the cage structure).[25] The Al atoms in this second peak are predominantly four coordinated, as shown in the 334 system in Figure 4, thus requiring charge compensation by the Ca. So the first adsorbed Ca layer charge compensates the tetrahedral Al in the terminal plane of the original crystal and the undercoordinated O in the crystal surface[23,26,28] as well as the Al in the second adsorbed peak.

The results also indicate that the Ca ions are inhibiting Al adsorption onto the basal surface. With less Ca in the IGF, the first adsorbed Ca peak is decreased and the first adsorbed Al peak is increased (123, 121, and 141 compositions).

Figure 3 also clearly shows that behavior is quite different in the 141 system. Here, the peak of the first Al adsorbed from the IGF onto the basal-oriented crystal has a density nearly that of the terminal Al layer in the crystal, and the first adsorbed Ca peak is missing. At this composition, with $R \ll R_e$, the Ca ions remain in the IGF to charge compensate the Al, with excess Al moving to both interfaces. In addition, in the 141 composition, the next adsorbed Al peak on the basal side has a shoulder and the beginning of a splitting of the peak, consistent with the double Al peak of the crystal with this orientation. The implication is that the 141 composition enables growth of the basal crystal along its surface normal in the [0001] direction because R is so low. In the current version of the simulation protocol, it would be expected that eventually enough Al would be removed from the glassy IGF to lower R to the point where its behavior is similar to the other compositions and adsorption (growth) slows. Of course, in a real system, a supply of ions from a source, such as dissolving alumina grains or a triple point, could offset this depletion process.

On the prism side, O from the IGF appropriately adsorbs initially, followed by a strong Al peak that grows to nearly equal that in the crystal. In the 141 composition, the strong first O and first Al peaks are followed by the next adsorbed O peak,

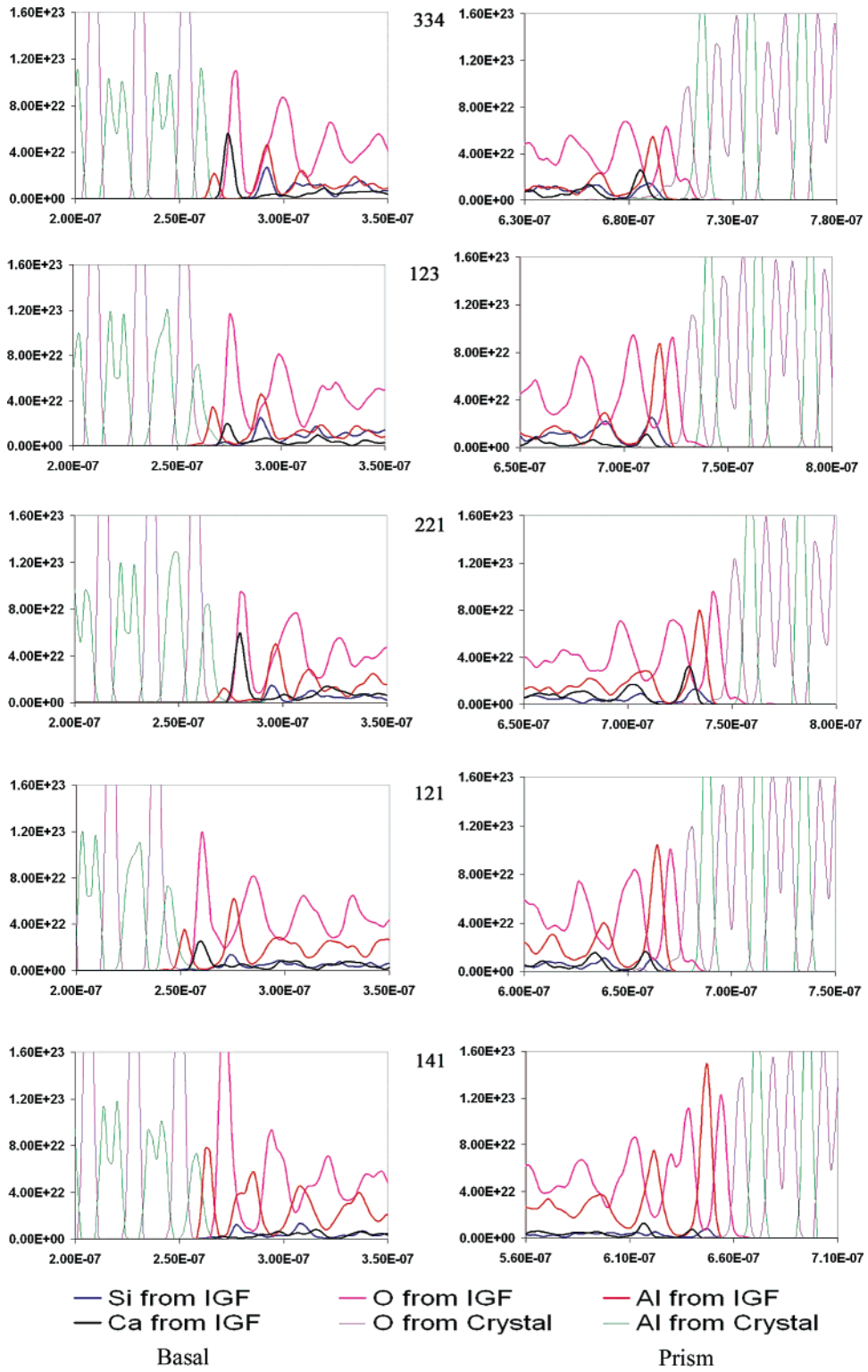

Figure 3. Density profiles of individual species at the basal and prism sides of the IGF for the five compositions as a function of distance perpendicular to the IGF−crystal interface. Thicker lines are for ions in the IGF. Line color associated with atom type is shown at the bottom of the figure.

which shows a splitting consistent with continuation of the crystal structure with this orientation. Ca has little effect on adsorption and growth on the prism side.

Therefore, the simulations show that Ca ions inhibit growth on the basal surface for most compositions but have little or no effect on the prism surface. This effect will be discussed more fully below.

Coordination Number Analysis. The coordination numbers (CNs) of Al and O are distinctly different in α-Al_2O_3 vs the alumino-silicate glass (the Si are four coordinated). The CNs of Al and O in the α-Al_2O_3 crystal are 6 and 4, respectively. In alkali and alkaline earth alumino-silicate glasses, Al is tetrahedrally coordinated and, depending on the alkali or alkaline earth-to-Al ratio, O is a mix of two coordinated (bridging oxygen), one coordinated (nonbridging oxygen), or three coordinated. The coordination of Al and O as a function of distance perpendicular to the IGF/crystal interfaces is shown in Figure 4 for two systems (334 and 141). The main features are that the Al and O in the IGF are predominantly four and two coordinated, as expected in the glass, with higher coordina-

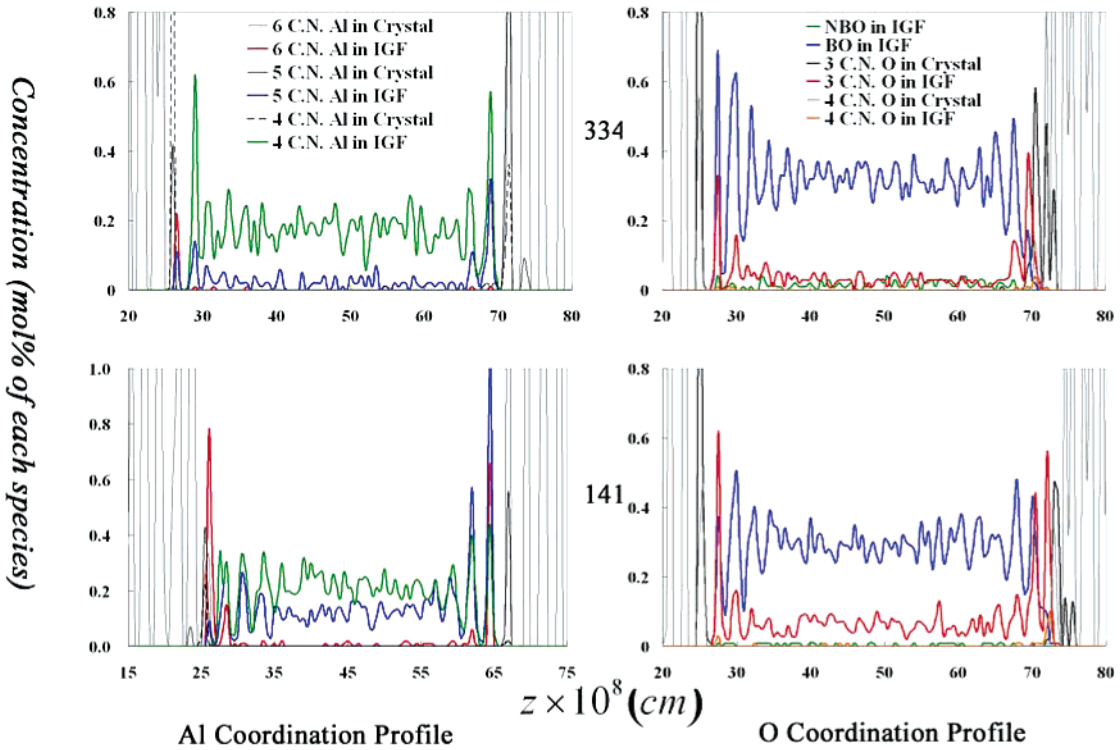

Figure 4. Coordination of Al and O species in the IGF and crystal surfaces for two compositions. Note the different scale of the concentrations in the Al profile in the 141 system. Al and O are predominantly four and two coordinated, respectively, in the IGF, as expected for the glass, with increasing coordination at the interfaces, consistent with the higher coordination of each in the crystal.

tion for each at the interfaces, which is consistent with the higher coordination of each in the crystal. Also, with significant excess of Al in the IGF (the 141 system), the coordination of Al and O increases in the glassy interior of the IGF. The correlation between coordination number of Al and O in alkali aluminosilicate glasses as a function of modifier content has been previously discussed,[22,39,40] with coordinations similar to those shown here. The increased coordination of Al and O in the glassy part of the IGF indicates a strain instability in the glass in comparison to a four-coordinated Al charge compensated by Ca and normal two-coordinated O that would be consistent with the network structure of a silicate glass. The implication is that Al (and O) should segregate to the interfaces to reduce the strain sites in the IGF when the *R* value is low. Another implication is that with sufficiently low Si content, the silicate glass structure might not dominate the IGF and a crystalline aluminate might form.

Relationship between the Crystal Growth and the Al Content in IGF. Figure 5 shows the integrated intensity of the first adsorbed Al peak on each interface normalized by the integrated intensity of the Al peak in the appropriately oriented crystal as a function of the ratio of Al ions to the sum of all cations. Included in the figure are the data from the IGF systems previously reported.[24] The normalized integrated intensity of the first adsorbed Al peak onto the crystal surface is used as an indicator of growth of the crystal. As mentioned above, "growth" here means adsorption of species from the IGF onto the crystal surface consistent with the crystal orientation and composition such that the crystal lattice extends along the surface normal of the particular plane in contact with the IGF. The results clearly show more rapid growth along the [11$\bar{2}$0] direction on the prism-oriented crystal than along the [0001] direction of the basal-oriented crystal, except at the highest Al concentration in the IGF. This difference in growth behavior is consistent with anisotropic grain growth observed experimentally in this system. In anisotropic grain growth in the alumina system, growth along

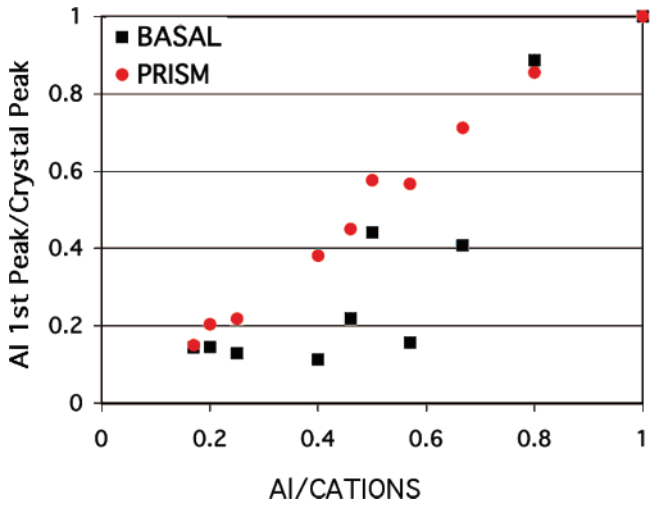

Figure 5. Normalized area under the first adsorbed Al peak from the IGF onto the different crystal surfaces as a function of the ratio of Al/all cations for the compositions presented here and the four compositions previously studied (see ref 24). Note the significantly faster growth along the prism surface normal than the basal surface normal for most compositions, except at the lowest and highest Al ratios.

the prism surface normal is much faster than that along the basal surface normal. Clearly, over most of the compositions used here, growth along the prism surface normal is 2−4 times faster than that on the basal surface.

At sufficiently high concentrations of Al in the IGF, near 0.8, growth along the basal surface normal is equivalent to that on the prism surface, indicating isotropic grain growth. That is, when the composition within the IGF has a sufficiently large concentration of Al present, Al and O ions adsorb onto both crystal surfaces epitaxially and extend the crystal dimension out in the direction of each surface normal. At this 141 composition, there is clearly a large excess of Al in comparison to Ca,

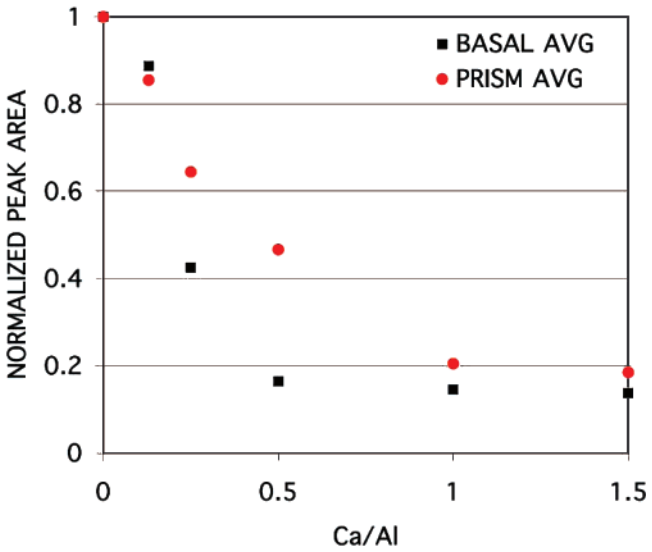

Figure 6. Average normalized area under the first adsorbed Al peak from the IGF onto the different crystal surfaces as a function of the Ca/Al ratio (R) for the compositions presented here and the four compositions previously studied (see ref 24). The equivalence point, R_e, is at 0.5. Below R_e, excess Al in the IGF allows for more rapid adsorption of Al onto the basal surface than that above the equivalence point.

allowing for more Al to adsorb onto the crystal sites before the Ca/Al ratio gets too high and inhibits continued growth. Therefore, with a sufficient supply of Al in the IGF, isotropic growth would be expected as Al adsorbs equally onto both basal- and prism-oriented crystal surfaces.

The data point at 0.5 Al/all cations (from the 123 system) and the two data points on either side (the 334 and 221) were reproduced in additional simulations with only minor variance, indicating something significant occurring at this specific composition. The 123 data point on the basal side is approximately the same as the value in the 121 system (seen at 0.66 Al/all cations). While the concentration of Si increases from the 121 to the 123, the R value remains the same. Considering the effect of the Ca/Al ratio (R) on the normalized adsorbed Al peak intensities provides clarification.

Figure 6 shows the plot of the adsorbed Al peak intensities, normalized by the crystal peak intensities, and averaged over equivalent R values in the IGFs, as a function of the Ca/Al ratio, R. The results clearly show that with $R \gg 0.5$, little Al adsorbs onto the surfaces, although slightly more Al adsorbs onto the prism surface. At $R \sim 0.5$, Al adsorption onto the prism surface increases significantly, with little change on the basal surface, indicating anisotropic grain growth. With $R < R_e$, adsorption onto the basal surface increases until it attains the same relative peak intensity as the prism surface at the lowest R value used here. At this lowest R value composition, isotropic growth is expected. The results imply grain growth would be most anisotropic near the equivalence point $R = 0.5$ and the most isotropic at very high and very low R values.

While crystal growth is complicated and depends on a variety of complex behavior, including dissolution of small grains or high energy surfaces, lattice vs grain boundary transport, reprecipitation, local stresses and strains, etc., the results shown here indicate the important role of the composition of the IGF on local behavior on prism and basal surfaces under the exact same conditions. Most importantly, the results show anisotropy in growth consistent with experimental observations, where growth along the basal surface normal is much slower than that on the prism surface normal, creating a platelet alumina structure.

Conclusions. Molecular dynamic simulations show the effect of the composition of the intergranular film (IGF) between dissimilarly oriented α-Al_2O_3 crystals on growth in the direction of each surface normal. The IGF in contact with the alumina (0001) basal plane on one side and the $(11\bar{2}0)$ prism plane on the other showed preferential growth in the $[11\bar{2}0]$ direction at all but the highest and lowest Ca/Al ratios in the IGF. Anisotropic grain growth in alumina is observed experimentally as excessive growth along the prism surface normal in comparison to the basal surface normal, creating platelet morphology. These simulations are consistent with such results and indicate the mechanism by which growth on the basal plane is inhibited, affecting growth. The role of Ca in the IGF is important and affects growth on the basal plane by poisoning surface sites based on the attraction of the Ca to charge compensate O on and adjacent to the basal surface. At Ca/Al ratios $\gg$0.5, which is the charge equivalence ratio, Al adsorption onto both surfaces is similar, but low, indicating slow isotropic growth. At Ca/Al ratios $\ll$0.5, Al adsorption is also similar on both surfaces, but fast, again indicating isotropic growth. Between these extreme Ca/Al ratios in the IGF, growth along the surface normal of the basal plane is inhibited in comparison to that on the prism plane, indicating anisotropic grain growth.

Acknowledgment. The authors acknowledge support from the DOE OBES, Division of Materials Sciences, Grant No. DE-FG02-00ER45823.

References and Notes

(1) Kaysser, W. A.; Sprissler, M. *J. Am. Ceram. Soc.* **1987**, *70*, 339.
(2) Powell-Dogan, C. A.; Heuer, A. H. *J. Am. Ceram. Soc.* **1990**, *73*, 3670.
(3) Powell-Dogan, C. A.; Heur, A. H.; O'Bryan, H. M. *J. Am. Ceram. Soc.* **1994**, *77*, 2593.
(4) Bae, S. I. *J. Mater. Sci.* **1993**, *28*, 4197.
(5) Bae, J.-S.; Pyun, S.-I. *J. Alloys Compd.* **1995**, *217*, 52.
(6) Bae, S. I.; Baik, S. *J. Am. Ceram. Soc.* **1993**, *76*, 1065.
(7) Jung, J.; Baik, S. *J. Am. Ceram. Soc.* **2003**, *86*, 644.
(8) Baik, S. *J. Am. Ceram. Soc.* **1988**, *71*, 358.
(9) Baik, S.; White, C. L. *J. Am. Ceram. Soc.* **1987**, *70*, 682.
(10) Kaplan, W. D. *J. Am. Ceram. Soc.* **1995**, *78*, 2841.
(11) Bae, S. I.; Baik, S. *J. Am. Ceram. Soc.* **1994**, *77*, 2499.
(12) Baik, S.; Moon, J. H. *J. Am. Ceram. Soc.* **1991**, *74*, 819.
(13) Park, C. W. *J. Am. Ceram. Soc.* **2003**, *86*, 603.
(14) Kolar, D. Discontinuous Grain Growth in Multiphase Ceramics. In *Sintering of Advanced Ceramics*; Handwerker, C. A., J. E. B., Eds.; American Ceramic Society: Westerville, OH, 1990; Vol. 7.
(15) Cho, S.-J.; Lee, Y.-C.; Lee, H.-L.; Sim, S.-M.; Yanagisawa, M. *J. Eur. Ceram. Soc.* **2003**, *23*, 2281.
(16) Lee, S.-H. *J. Eur. Ceram. Soc.* **2002**, *22*, 317.
(17) Kwon, O.-S.; Hong, S.-H.; Lee, J.-H.; Chung, U.-J.; Kim, D.-Y.; Hwang, N. M. *Acta Mater.* **2002**, *50*, 4865.
(18) Ziegler, A.; Kisielowski, C.; Hoffmann, M. J.; Ritchie, R. O. *J. Am. Ceram. Soc.* **2003**, *86*, 1777.
(19) Shibata, N.; Pennycook, S. J.; Gosnell, T. R.; Painter, G. S.; Shelton, W. A.; Becher, P. F. *Nature* **2004**, *428*, 730.
(20) Doblinger, M.; Winkelman, G. B.; Dwyer, C.; Marsh, C.; Kirkland, A. I.; Cockayne, D. J. H.; Hoffmann, M. J. *Acta Mater.* In press.
(21) Clarke, D. *J. Am. Ceram. Soc.* **1987**, *70*, 15.
(22) Zirl, D. M.; Garofalini, S. H. *J. Am. Ceram. Soc.* **1990**, *73*, 2848.
(23) Blonski, S.; Garofalini, S. H. *J. Am. Ceram. Soc.* **1997**, *80*, 1997.
(24) Zhang, S.; Garofalini, S. H. *J. Am. Ceram. Soc.* **2005**, *88*, 202.
(25) Litton, D. A.; Garofalini, S. H. *J. Mater. Res.* **1999**, *14*, 1418.
(26) Litton, D. A.; Garofalini, S. H. *J. Am. Ceram. Soc.* **2000**, *83*, 2273.
(27) Garofalini, S. H.; Luo, W. *J. Am. Ceram. Soc.* **2003**, *86*, 1741.
(28) Garofalini, S. H.; Zhang, S. In *Materials Research Society Symposium Proceedings*; Materials Research Society: Pittsburgh, PA, 2003; Vol. 751, p 191.
(29) Blonski, S.; Garofalini, S. H. *J. Phys. Chem.* **1996**, *100*, 2201.
(30) Blonski, S.; Garofalini, S. H. *Surf. Sci.* **1993**, *295*, 263.

(31) Delaye, J.-M.; Louis-Achille, V.; Ghaleb, D. *J. Non-Cryst. Solids* **1997**, *210*, 232.
(32) Feuston, B. P.; Garofalini, S. H. *J. Chem. Phys.* **1988**, *89*, 5818.
(33) Litton, D. A.; Garofalini, S. H. *J. Non-Cryst. Solids* **1997**, *217*, 250.
(34) Mackrodt, W. C.; Davey, R. J.; Black, S. N.; Docherty, R. *J. Cryst. Growth* **1987**, *80*, 441.
(35) Batirev, I. G.; Alavi, A.; Finnis, M. W.; Deutsch, T. *Phys. Rev. Lett.* **1999**, *82*, 1510.
(36) Garofalini, S. H. *J. Non-Cryst. Solids* **1990**, *120*, 1.
(37) Garofalini, S. H. In *Reviews in Mineralogy and Geochemistry: Molecular Modeling Theory: Applications to the Geosciences*; Cygan, R., Kubicki, J., Eds.; Mineralogical Society of America: Washington, DC, 2001; Vol. 42, p 131.
(38) Feuston, B. F.; Garofalini, S. H. *J. Chem. Phys.* **1989**, *91*, 564.
(39) Huang, C.; Cormack, A. N. *J. Chem. Phys.* **1990**, *93*, 8180.
(40) Huang, C.; Cormack, A. N. *J. Chem. Phys.* **1991**, *95*, 3634.